Centrality dependence of the expansion dynamics in Pb-Pb collisions at 158 A GeV/c

The WA97 Collaboration:
F Antinori[9], W Beusch[5], I J Bloodworth[4], G E Bruno[1], R Caliandro[1], N Carrer[9], D Di Bari[1], S Di Liberto[11], D Elia[1], D Evans[4], K Fanebust[2], F Fayazzadeh[8], R A Fini[1], B Ghidini[1], G Grella[12], H Helstrup[3], M Henriquez[8], A K Holme[8], A Jacholkowski[1], G T Jones[4], J B Kinson[4], K Knudson[5], I Králik[6], V Lenti[1], R Lietava[6], R A Loconsole[1], G Løvhøiden[8], V Manzari[1], M A Mazzoni[11], F Meddi[11], A Michalon[13], M E Michalon-Mentzer[13], M Morando[9], P I Norman[4], B Pastirčák[6], E Quercigh[5], D Röhrich[2], G Romano[12], K Šafařík[5], L Šándor[5,6], G Segato[9], P Staroba[10], M Thompson[4], J Urbán[6], T Vik[8], O Villalobos Baillie[4], T Virgili[12], M F Votruba[4] and P Závada[10].

[1] Dipartimento I.A. di Fisica dell'Università e del Politecnico di Bari and Sezione INFN, Bari, Italy
[2] Fysisk institutt, Universitetet i Bergen, Bergen, Norway
[3] Høgskolen i Bergen, Bergen, Norway
[4] School of Physics and Astronomy, University of Birmingham, Birmingham, UK
[5] CERN, European Laboratory for Particle Physics, Geneva, Switzerland
[6] Institute of Experimental Physics, Slovak Academy of Sciences, Košice, Slovakia
[7] GRPHE, Université de Haute Alsace, Mulhouse, France
[8] Fysisk institutt, Universitetet i Oslo, Oslo, Norway
[9] Dipartimento di Fisica dell'Università and Sezione INFN, Padua, Italy
[10] Institute of Physics, Academy of Sciences of Czech Republic, Prague, Czech Republic
[11] Dipartimento di Fisica dell'Università "La Sapienza" and Sezione INFN, Rome, Italy
[12] Dipartimento di Scienze Fisiche "E.R. Caianiello" dell'Università and INFN, Salerno, Italy
[13] Institut de Recherches Subatomiques, IN2P3/ULP, Strasbourg, France

Abstract. Two-particle correlation functions of negatively charged hadrons from Pb-Pb collisions at 158 GeV/c per nucleon have been measured by the WA97 experiment at the CERN SPS. A Coulomb correction procedure that assumes an expanding source has been implemented. Within the framework of an expanding thermalized source model the size and dynamical state of the collision fireball at freeze-out have been reconstructed as a function of the centrality of the collision. Less central collisions exhibit a different dynamics than central ones: both transverse and longitudinal expansion velocities are slower, the expansion duration is shorter and the system freezes out showing smaller dimensions and higher temperature.

Submitted to: *JPG*

PACS numbers: 25.75.Gz, 25.75.Ld

1. Introduction

The study of ultrarelativistic heavy ion collisions is motivated mainly by the QCD predictions that at sufficiently high energy density the excited nuclear matter undergoes a phase transition into a system of deconfined quarks and gluons (Quark–Gluon Plasma: QGP).

The most direct measurement of space-time characteristics of the collision region is provided by Hanbury-Brown and Twiss (HBT) interferometry, a method developed originally in astronomy in the fifties [1] and applied independently in the field of particle physics a few years later [2].

Over the last years this method has been widely used in ultrarelativistic heavy collisions to investigate the space-time geometry of the source, and ample evidence accumulated showing that information can be gained both on its geometry and its dynamics. For a recent review see e.g. [3].

In ref. [4, 5] an analysis strategy for reconstructing the freeze-out source state in heavy-ion collisions was suggested. A model for an emitting source characterized by a collective flow dynamics superimposed to a random (thermal) motion was assumed therein. The parameters of the model are the freeze-out temperature T, the transverse geometric (Gaussian) radius $\sqrt{2}R_G$, the average freeze-out proper time τ_0, the mean proper time duration of particle emission $\Delta\tau$, the transverse flow velocity $\beta_\perp$, and $\Delta\eta$, that parametrizes the longitudinal extension of the source.
This approach has been followed by the NA49 experiment, that has reconstructed the freeze-out state for very central Pb-Pb collisions (about 3% of the most central events) at 158 GeV per nucleon [6].

In this paper we also follow the model of ref. [4, 5], but in addition we evaluate all the source parameters as a function of centrality, owing to the relatively large centrality window explored by the WA97 experiment.

The correlation analysis presented here is based on pairs of negative hadrons (h^-), which are dominated by pairs of identical pions. Misidentified particles lead to counting of unlike pairs which do not give rise to Bose-Einstein correlation. It has been shown in [7, 8] (NA35 exp.) and in [6] (NA49 exp.) that the main effect of particle misidentification is to reduce the value of the chaoticity parameter λ, which, however, is not used for the reconstruction of the size and dynamical state of the source; the relevant source parameters are effected by a few percents only. Moreover in this paper we present a compilation of recent results from other SPS experiments, which use either unidentified h^--h^- pairs (NA49 [6], WA98 [9]) or π^--π^- pairs (NA44 [10]); their agreement supports the assumption that HBT correlation can be performed using h^--h^- pairs.

The paper is structured as follows: the WA97 apparatus is briefly described in section 2. The experimental derivation of the two-particle correlation function is discussed in section 3; section 4 deals with the Coulomb corrections. In section 5 the measured radii are presented as a function of the pair momentum; from them

the source freeze-out size and temperature, the average freeze-out time and duration, and the expansion velocity are derived as functions of the collision centrality. From these observables a dynamical picture of the collision is depicted in section 6. Finally conclusions are drawn in section 7.

2. The WA97 experiment

The WA97 set-up, shown schematically in fig. 1, is described in detail in ref. [11]. The target and the silicon telescope were placed inside the homogeneous 1.8 T magnetic field of the CERN Omega magnet. The 158 A GeV/c lead beam from the CERN SPS was

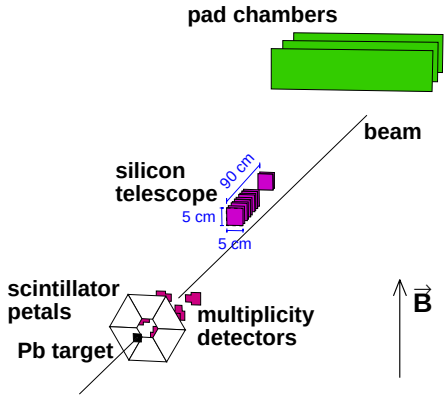

Figure 1. The WA97 set-up.

incident on a lead target with a thickness corresponding to 1% of an interaction length. Scintillator petal detectors behind the target provided an interaction trigger selecting approximately the most central 40% of the Pb-Pb collisions. Two planes of microstrip multiplicity detectors covering, for all p_T values, the pseudorapidity region $2 \lesssim \eta \lesssim 3$ and $3 \lesssim \eta \lesssim 4$ respectively, provided information for more detailed off-line study of the centrality dependence of single and double particle spectra. In the present analysis the WA97 usual four centrality bins, described in ref. [12, 13] for the study of strangeness production, have been adopted.

The core of the WA97 set-up is a silicon telescope consisting of 7 planes of pixel detectors [14] which have a pixel size of $75 \times 500\,\mu\mathrm{m}^2$ and of 10 planes of $50\,\mu$m pitch silicon microstrips. The telescope has $5 \times 5\,\mathrm{cm}^2$ cross section and contains $\approx 0.5 \times 10^6$ detecting elements. This precise tracking device was placed 60 cm behind the target slightly above the beam line and inclined by 48 mrad, pointing to the target.

The track reconstruction is done in the compact part of the telescope, where 11 planes of silicon detectors are closely packed over a distance of 30 cm. The momentum resolution for fast tracks is improved using lever arm detectors, which consists of additional pixel and microstrip planes and of three MWPC's with a cathode pad readout. Due to the precise tracking and to its compactness the WA97 experiment is well suited for the measurements of the two-particle correlation functions.

3. Data analysis

The quantum statistical correlation between two identical particles coming from a chaotic source yields information on the dimensions and the dynamics of the source. Experimentally the correlation is studied through a "correlation function", defined as:

$$C_2(q) = \mathcal{N}\frac{S(q)}{B(q)} \tag{1}$$

where $S(q)$ is the measured two-particle (Signal) distribution as a function of the relative four momentum $q = p_1 - p_2$ and $B(q)$ is the reference (Background) distribution built by pairing two particles taken from different events. For each actual pair in one event (in the Signal) about 50 background pairs have been formed from events of similar multiplicity, so that the statistical error on C_2 is dominated by the signal. The normalization factor $\mathcal{N}$ is determined by imposing that the integral of $C_2(q)$ over a wide interval outside the region of sensitive correlation (which is at low q) is equal to one.

From the correlation function C_2 the description of the source has been extracted using two different parametrizations.

(1) The "standard" Cartesian (or Pratt-Bertsch) parametrization [15, 16] is expressed in the *out-side-longitudinal* (OSL) system; this has the *longitudinal* direction along the beam axis, while in the transverse plane the *out* direction is chosen parallel to the transverse component of the pair momentum $\vec{K}_t$, the remaining Cartesian component denoting the *side* direction. This parametrization is given by the following formula:

$$C_2(q) = 1 + \lambda \exp\left[-R_o^2 q_o^2 - R_s^2 q_s^2 - R_l^2 q_l^2 - 2|R_{ol}|R_{ol} q_l q_o\right] \tag{2}$$

where q_o, q_s, q_l are the spatial components of q in the OSL system and R_o, R_s, R_l, R_{ol}, which are fit parameters, provide information on the extension and dynamics of the source [16]. λ is called the "chaoticity parameter" and is equal to unity for a completly chaotic source and smaller than unity for partially chaotic source. It is however affected in a non trivial way by resonance decays, particle misidentification and other effects [17], which are expected to depend on the pair momentum.

(2) The Yano-Koonin-Podgoretskii (YKP) parametrization [18] uses the components $q_\perp = \sqrt{q_o^2 + q_s^2}$, $q_0 = E_1 - E_2$, $q_\parallel = q_l$ and starts from the ansatz:

$$C_2(q) = 1+\lambda \exp\left[-R_\perp^2 q_\perp^2 - \gamma_{yk}^2 (q_\parallel - v_{yk} q_0)^2 R_\parallel^2 - \gamma_{yk}^2 (q_0 - v_{yk} q_\parallel)^2 R_0^2\right] \tag{3}$$

where $R_\perp$, $R_\parallel$, R_0 are called the "YKP radii", although R_0 has temporal dimension (fm/c); v_{yk}, called "Yano-Koonin velocity", is measured in units of c and $\gamma_{yk} = (1 - v_{yk}^2)^{-1/2}$.

The transverse orientation of the reference system is different in the two parametrizations. Concerning the longitudinal direction, the LCMS (*longitudinal co-moving system*) frame, in which the average pair momentum has only a transverse component ($K_l = 0$), has been chosen for both of them. This system has the advantage of a more straightforward interpretation of the source parameters. Hence, a reference

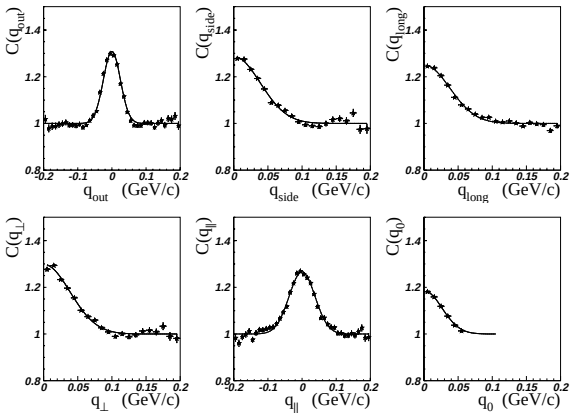

Figure 2. Projections of the h^--h^- correlation function measured using Cartesian (top) and YKP (bottom) parametrization for pair rapidities $2.55 < Y_{\pi\pi} < 3.65$ and pair trasverse momenta $0.23 < K_t < 0.39\,\mathrm{GeV}/c$. Solid curves are the result of a least-square fit to a Gaussian function (see the text).

system is used where the relative momentum q is measured on a pair-by-pair basis. The same is true in the transverse direction for the Cartesian parametrization.

As claimed in ref. [19], fitting by the Least Square method and using the square root of the number of counts as an estimator of the error introduces a systematic bias. A Maximum Likelihood method has been applied by minimizing the negative logarithmic likelihood function:

$$-2\ln\mathcal{L}(\vec{R}) = 2\sum_i \left[C_i B_i - S_i \ln(C_i B_i) + \ln(S_i!)\right] \tag{4}$$

where C_i is the correlation hypothesis for a given set of fit parameters $\vec{R}$ (e.g. $\vec{R} = (\lambda, R_\perp, R_\parallel, R_0, v_{yk})$).

The main quality test of the full analysis procedure comes from the consistency between parameters obtained from Cartesian and YKP forms of the correlation function. This topic is discussed in section 5. Two secondary checks on the fit quality have been performed. Firstly, the χ^2/NDF–values are calculated for the parameters corresponding to the best likelihood fits and are found to be distributed around unity. Secondly, we have fitted the projections of the 3-dimensional correlation functions onto one momentum difference component, with narrow cuts on the other components, using a least-squares method to a Gaussian function. This yields results consistent with the results of the 3-dimensional fits. A typical sample of these projections is shown in fig. 2 where the correlation function has been integrated along the other q_j components in the intervals $|q_j| < 20\,\mathrm{MeV}$, except for the $q_0 = E_1 - E_2$ projection where $|q_j| < 50\,\mathrm{MeV}/c$ ($j = \perp, \parallel$).

The determination of the size and dynamical state of the source at freeze-out requires information about the dependence of the YKP radii on the mean momentum $\vec{K} = \frac{1}{2}(\vec{p}_1 + \vec{p}_2)$ of the pair. This can be parametrized by its transverse component $K_t = \frac{1}{2}\sqrt{(p_{y1}+p_{y2})^2 + (p_{z1}+p_{z2})^2}$ and the pair rapidity $Y_{\pi\pi} = \frac{1}{2}\log\frac{E_1+E_2+p_{x1}+p_{x2}}{E_1+E_2-p_{x1}-p_{x2}}$.

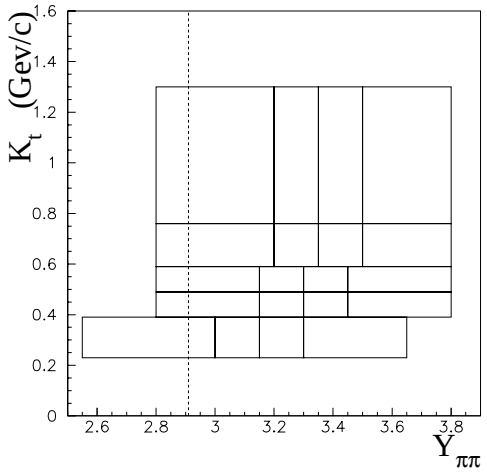

Figure 3. Two-particle acceptance window (assumed to be pions) used in the present analysis. The correlation function has been measured in each of the twenty rectangles patching the window together. The K_t and $Y_{\pi\pi}$ average values, measured over the rectangles are reported in table 1. The dashed line is drawn at $Y_{\pi\pi} = y_{cm}$.

With this in mind, our (two-particle) acceptance window, which is shown in fig. 3, has been binned in 20 rectangles in each of which the correlation function $C_2(q)$ has been measured independently. Table 1 displays the average values of the K_t and $Y_{\pi\pi}$ distributions in each of the 20 bins used for the analysis.

Table 1. Averages of the K_t (uppermost number in the cells, in GeV/c units) and $Y_{\pi\pi}$ (bottom numbers) distributions in the 20 rectangles of fig. 3.

	$Y_{\pi\pi} \longrightarrow$			
	0.910	0.915	0.915	0.925
	3.11	3.28	3.42	3.60
	0.660	0.665	0.665	0.670
	3.10	3.28	3.42	3.60
$\uparrow$	0.535	0.535	0.540	0.540
	3.05	3.23	3.37	3.56
K_t	0.435	0.440	0.440	0.445
	3.03	3.23	3.37	3.55
	0.315	0.330	0.335	0.345
	2.86	3.08	3.22	3.42

Additionally, in order to investigate the dynamics of the collisions as a function of centrality, the whole analysis has been repeated for each of the four centrality classes selected by WA97 to study the strange particle production [12, 13].

The quality of a correlation measurement is determined by the resolution of the two-particle momentum difference ("relative momentum") q. The relative momentum

resolution was studied using a Monte Carlo chain based on the simulation code GEANT [20]. As reported in table 2, we have found that all relative momentum projections used in this analysis (q_o, q_s, q_l; $q_\perp$, $q_\parallel$, q_0) are measured with an error not bigger than 10 MeV/c over our two-particle acceptance window.

Table 2. The resolution of relative momenta q_o, q_s, q_l and $q_\perp, q_\parallel, q_0$ in the LCMS frame.

Projection	Resolution (MeV/c)
q_o	7.5
q_s	10
q_l	7.5
$q_\perp$	9.0
$q_\parallel$	7.5
q_0	7

The bin size used to build the correlation functions has been accordingly taken to be 10 MeV/c in all relative momentum components. It has been shown in [21] that due to the finite bin size the values of the extracted HBT radii are systematically underestimated, the greater the radius the higher the error. Since the typical half-width of the correlation function in our acceptance window is ~ 50 MeV/c (corresponding to a typical radius of about 4 fm), our binning yields an underestimation smaller than 10%.

The detector's ability to distinguish a pair of close tracks from a single track decreases with decreasing track separation, depending on the Si-pixel size. The correction for this inefficiency was calculated via a Monte Carlo simulation by reconstructing a sample of (generated) two-tracks events embedded in real ones. The maximum inefficiency was found to be $\approx$ 4% for pairs populating the bin of the correlation functions centred at $q = 0$ (relative to high q pairs).

The results presented here are based on 17 million events collected in the 1995 run. Only tracks pointing to the main interaction vertex, which is reconstructed on a event by event basis, are selected. After event reconstruction we end up with 13 million h^- pairs in the correlation sensitive region $|\vec{q}| < 100$ MeV/c (LCMS system).

4. Coulomb correction

The observed two-particle correlation is the result of two different contributions, the Bose-Einstein effect and the Coulomb interactions. The Coulomb interaction between the particles of a pair accelerates them relative to each other, thus depleting the two-particle correlation function at small relative momenta.

In order to get the Bose-Einstein correlation alone, the correlation function C_2 needs to be corrected for the Coulomb interaction among the particles, so that:

$$C_2(p_1, p_2) = C_2^{raw}(p_1, p_2) \times K_{Coul}(p_1, p_2) \tag{5}$$

where C_2^{raw} is the B-E correlation of the experimental data and K_{Coul} is the correction for the Coulomb interaction. In the past, the correction was done by describing the emission of an isolated pairs of charged particles from a point-like neutral region (Gamow factor [22, 23]). This correction has been shown to be inadequate in heavy ion collision at the SPS energy [24, 25], essentially due to the extent of the source which is far from a point-like approximation. The Gamow factor has been considered in this analysis just as a reference for the two correction methods implemented. Those are:

i) The method based on the measure of oppositely charged particle correlation, following the approach of Baym and Braun-Munzinger [26].
Oppositely charged particles do not present correlation due to quantum statistical effects; they can thus provide a direct measure of the additional correlation introduced by the Coulomb interaction, accounting for the reverse in the charge sign. The method suggested in [26] is a classical model which neglects Coulomb interaction inside a pair for separations less then a given r_0 and includes it for larger separations. A charge screening effect, expected in the high multiplicity environment created just after an ultra-relativistic heavy ion collision, is thus taken into account. The only free parameter of the model, r_0, can be obtained by a fit to the measured data points of the correlator for oppositely charged particles. The obtained value, $r_0 = 6.1 \pm 0.5\,\mathrm{fm}$, is consistent with the NA49 measurement [6]. The resulting correction function is shown in fig. 4 as a function of $q_{inv} = \sqrt{\vec{q}^2 - q_0^2}$.

ii) The full Coulomb wave-function integration [27, 28]. This method has the advantage of being adaptable to any emission mechanism and can be implemented in bin-by-bin correction, independently of which particular projections of $q = p_1 - p_2$ are in use. Coulomb interactions with the residual nuclear system are neglected. As a validation test of the procedure, we first assumed a point-like source (i.e. very small volume, $<< 1\,\mathrm{fm}$) with sudden emission (i.e. the particles are emitted at the same time), comparing to the Gamow correction. The agreement is satisfactory as shown in fig. 4. Then two kinds of source have been implemented:
   (a) a Gaussian source with sudden emission, which has been traditionally used in connection with the wave-function integration.
   (b) the same source model adopted to investigate the features of the expansion dynamics and geometry of the fireball.
   Since the parameters of the model, namely T, $\beta_\perp$, $\mathrm{R_G}$, $\Delta\eta$, $\Delta\tau$, τ_0, are required to describe the source during the computation of the Coulomb correction, an iterative procedure has been followed:
      - a first complete analysis of the correlation functions corrected with the Baym and Braun-Munzinger approach, leads to a first estimate of the model parameters;
      - these parameters are used to calculate a new Coulomb correction by means of the full wave-function integration method;

- a second full analysis of the correlation with the new Coulomb correction (that will be presented in the next section) leads to a second, better evaluation of the model parameters.

The procedure converged satisfactorily after the second iteration.

A final comparison of all the methods is shown in fig. 4. As expected, the Gamow factor significantly overestimates the Coulomb interaction in heavy ion collision; the corrections calculated with the static Gaussian source and those of the Baym model, that implicitly also assumes a static source, are found to be very similar. The expanding source has proven to yield the smallest corrections. We may conclude that treating a rapidly expanding source as if it were a *static* system can lead to a slight overestimate of the Coulomb corrections. The correction has been applied on a bin-by-bin basis, acting

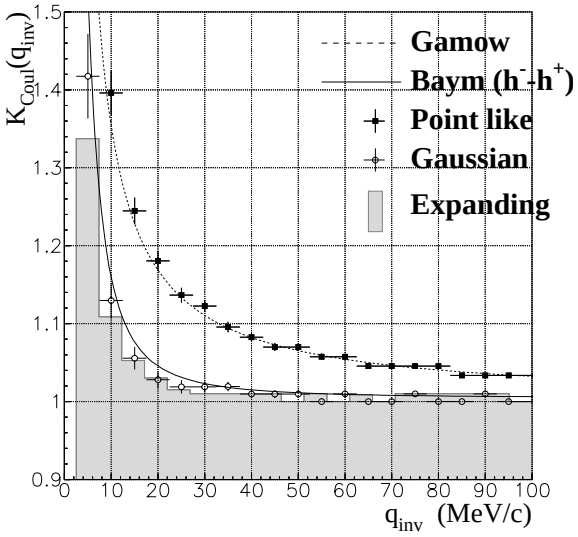

Figure 4. Corrections to the correlation function for the Coulomb interaction according different models: the Gamow factor (dashed line), the Baym method based upon the correlation of oppositely charged particles (solid line), the full wave-function integration for a point-like source (black squares) and for a (static) Gaussian source with rms radius of 4 fm (open circles), the full wave-function integration for an expanding thermalized source [5] (shadow area).

on the q_{inv} of that bin, even if we are making a correlation function in some other set of variables.

5. Correlation study

5.1. Cartesian and YKP parametrizations: consistency

In the context of the model by Chapman et al. [4] for a finite expanding thermalized source, the YKP parameters give more direct access to the features of the source. Therefore in this paper we shall follow this approach. However, the Cartesian

radii have been systematically used to test the goodness of the fitting procedure of the YKP correlation function, by means of equations relating the two sets of parameters (for these equations see e.g. [5, 29]). Fig. 5 shows typical fit results for the parameters $(\lambda, R_\perp, R_\parallel, R_0)$ versus K_t as obtained directly from YKP parametrization (black triangles) and deduced from the corresponding Cartesian set of parameters (open circles); as a second representative sample, in fig. 6 are displayed the Cartesian radii versus $Y_{\pi\pi}$ evaluated directly and from the corresponding YKP correlation functions. It is worth stressing that the analysis has been carried out in a completely independent way for the two parametrizations: this means, for instance, that the corrections for Coulomb interaction and two-track resolution have been calculated and applied independently. In short, Cartesian and YKP radii give two separate measurements of the same physical quantities; their full compatibility gives confidence on the absence of systematic errors in the analysis.

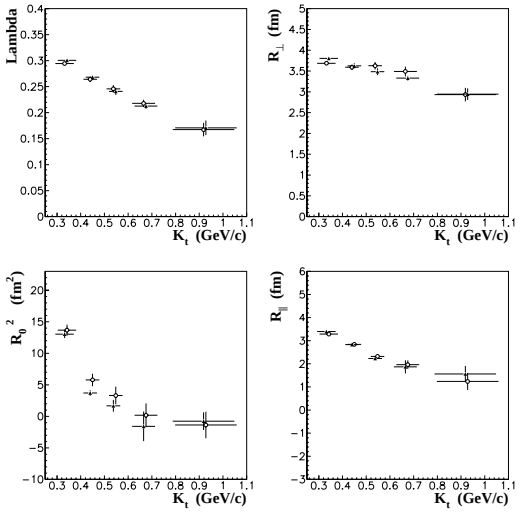

Figure 5. The λ factor and the YKP radii as calculated directly (black triangles) and from the Cartesian parametrization (open circles) as a function of K_t in the full $Y_{\pi\pi}$ and centrality interval. The remaining parameter v_{yk} is displayed in fig. 9 (plot labelled "ALL").

In fig. 7 we have compiled recent results from other CERN heavy-ion experiments, namely NA49 [6, 21, 30], WA98 [9] and NA44 [10], along with our results for the two most central collision classes (III and IV) merged together. The overall agreement of our data with the other experiments is convincing both in the common K_t region and when extrapolating to small K_t. WA97 is the sole experiment that explores the high K_t region and our data suggest a flattening of the $R_\perp$, $R_\parallel$, R_s and R_l behaviour with K_t at high values.

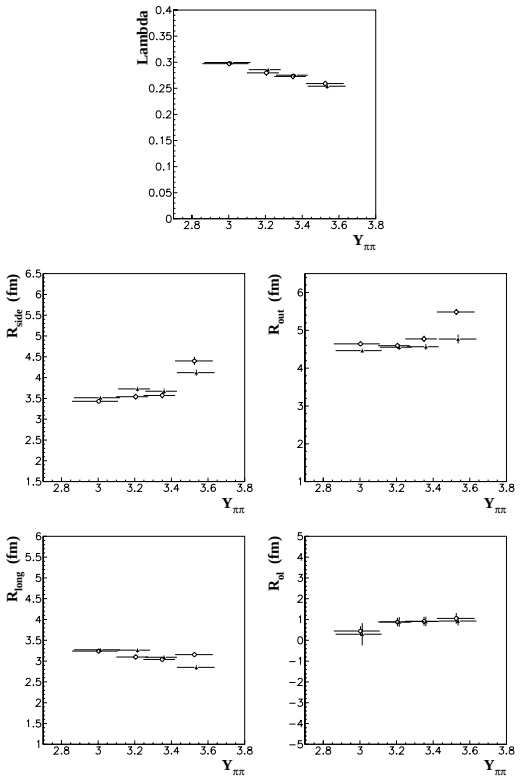

Figure 6. Cartesian parameters as calculated directly (open circles) and from the YKP parametrization (black triangles) as a function of $Y_{\pi\pi}$ in the interval $0.23 < K_t < 0.76\,\mathrm{GeV}/c$.

5.2. The Yano-Koonin velocity versus $Y_{\pi\pi}$: longitudinal flow

Fig. 8 shows the YK rapidity $Y_{YK} = \frac{1}{2}\log\frac{1+v_{yk}}{1-v_{yk}} + Y_{\pi\pi}$, calculated from the fitted parameter v_{yk}, as a function of the pair rapidity $Y_{\pi\pi}$ (both displayed in the laboratory system) separately for the four centrality classes and in the inclusive case (class "ALL"). The v_{yk} fit parameter is often determined with a larger relative error than $R_\perp$, $R_\parallel$ or λ (the same is true for R_0); therefore four data sets (in the K_t variable) have been merged in order to obtain small errors on v_{yk}.

As explained in ref. [5] the dependence of the YK rapidity on the pair rapidity should directly measure the longitudinal expansion of the source and cleanly separate it from its transverse dynamics. In particular, for a non-expanding source Y_{YK} would be independent of $Y_{\pi\pi}$ (horizontal lines in fig. 8), while for the case of a longitudinally expanding, boost-invariant source these variables would be completely correlated (diagonal lines in the same figure). It has been shown in ref. [29] that, as a consequence of the reduced thermal smearing at large K_t, the linear relation $Y_{YK} = Y_{\pi\pi}$ is better satisfied the larger the transverse momentum of the particle pair. Hence this linear relation cannot be generally interpreted as evidence for a true boost-invariant longitudinal expansion. The dependence of the YK velocity on K_t is expected however to be of minor importance.

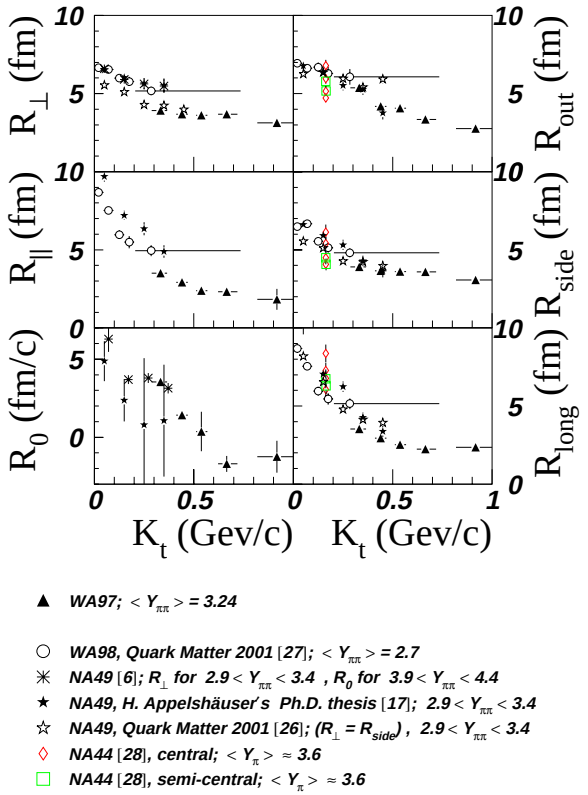

Figure 7. Dependence of the HBT radii on the transverse momentum of the pair for Pb-Pb collisions at SPS energy.

The results of fig. 8 thus would suggest that the source expands longitudinally in a nearly boost-invariant way for the three most central collision classes and with much less intensity for the most peripheral one. We observe, however, an unexpectedly *strong* dependence of v_{yk} (hence of Y_{YK}) on the transverse pair momentum K_t, as discussed in the next section.

5.3. The Yano-Koonin velocity versus K_t: v_{yk} positive and close to c at high K_t

Fig. 9 shows the K_t dependence of v_{yk} in the inclusive case of all centrality classes merged together (class "ALL"), and in the four centrality classes separately. In order to make a quantitative comparison of the behaviour of v_{yk} in the different classes, we have parametrized v_{yk} as a linear function of K_t: $v_{yk} = a + bK_t$. The slope b is found to be similar for all the four centrality classes with a value of about $1.5\,(\mathrm{GeV}/c^2)^{-1}$, while the value of the intercept a is different for class I ($a \approx -0.8\,c$) with respect to classes II,III and IV ($a \approx -0.6\,c$). The parametrization works satisfactorily up to $K_t \simeq 0.8\,\mathrm{GeV}/c$, but the linear approximation becomes unphysical ($v_{yk}/c > 1$) for $K_t > \frac{c-a}{b} \sim 1\,\mathrm{GeV}/c$, therefore a saturation of v_{yk} up to a value close to the speed of lighthas to be supposed.

Positive v_{yk} in the LCMS means that the diagonal lines of fig. 8 are crossed. Points

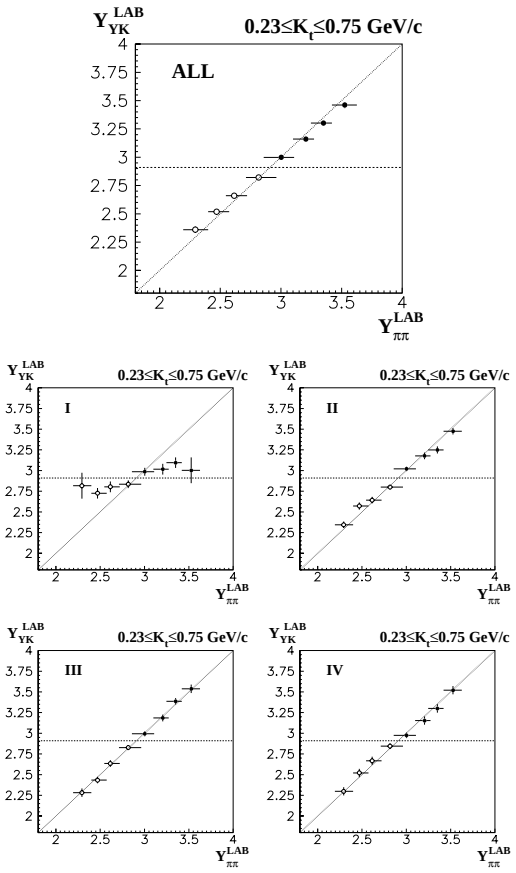

Figure 8. $Y_{\pi\pi}$ dependence of the YK rapidity for the four centrality classes and for the inclusive case (ALL). Class I corresponds to the most peripheral collisions and class IV to the most central ones. Filled circles are data, open circles are data reflected about mid-rapidity.

in fig. 8 are measured in the wide interval $0.23 < K_t < 0.75\,\mathrm{GeV}/c$, the average K_t over this interval being however $\simeq 0.45\,\mathrm{GeV}/c$. Since v_{yk} crosses the zero value for $K_t \sim 0.4\,\mathrm{GeV}/c$, looking back at fig. 8 we may claim that the experimental points are close to the 45^o-degree line mainly because of their (mean) K_t values. We can conclude that the slopes of the plots Y_{YK}^{SYS} versus $Y_{\pi\pi}^{SYS}$ (SYS being either LAB or CMS), often encountered in literature, are influenced *strongly* by K_t. Therefore no conclusive predictions on the longitudinal expansion can be drawn by looking solely at the $Y_{\pi\pi}$ dependence of the Yano-Koonin velocity. It is a fact, however, that we measure smaller v_{yk} for centrality class I: the a intercept has a larger negative value and the zero crossing occurs at higher K_t for this class. Since the mean K_t of the pairs is found to be the same over the four centrality classes, therefore it can be deduced a less intense longitudinal expansion for class I.

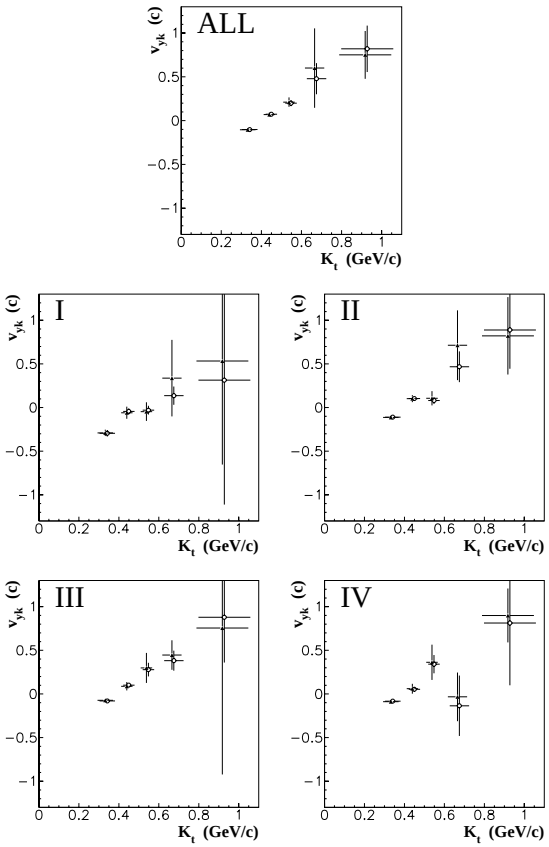

Figure 9. K_t dependence of the YK velocity in the four centrality classes and the inclusive (ALL) one. Black triangles are v_{yk}'s measured directly in the YKP parametrization, open circles are deduced from Cartesian radii.

5.4. The $R_\perp$ radius: transverse flow and temperature

While longitudinal "flow" is not necessarily a signature for nuclear collectivity, because it may be due simply to incomplete stopping of the two colliding nuclei, *transverse* collective expansion flow can only be generated by the build up of a locally isotropic pressure component. The transverse radius parameter $R_\perp$ is invariant under longitudinal boosts and thus is not affected at all by longitudinal expansion. It is expected to drop as a function of $M_t = \sqrt{m_\pi^2 + K_t^2}$ if the source expands in the transverse direction [4].

In ref. [4], in the context of a source model characterized by longitudinal and transverse expansion, the following expression for $R_\perp$ has been derived:

$$R_\perp(K_t, Y_{\pi\pi}) = R_G \left[1 + M_t \frac{\beta_\perp^2}{T} \cosh(Y_{YK} - Y_{\pi\pi})\right]^{-\frac{1}{2}} \tag{6}$$

where R_G is equal to the transverse geometric (Gaussian) radius of the source times $1/\sqrt{2}$, T is the freeze-out temperature and $\beta_\perp$ the slope of the (linear) transverse flow velocity profile: $\beta_\perp(r) = \beta_\perp \frac{r}{R_G}$. A bidimensional fit of function (6) to the experimental data has led to the determination of R_G and $\frac{\beta_\perp^2}{T}$. The fit results are summarized in table 3.

Table 3. The transverse geometric parameter R_G and the ratio $\beta_\perp^2/T$, T being the freeze-out temperature.

Centrality	R_G (fm)	$\frac{\beta_\perp^2}{T}$ (GeV^{-1})	χ^2/ndf
ALL	4.75 ± 0.38	1.62 ± 0.60	21.6/18
I	3.20 ± 0.31	0.68 ± 0.55	21.6/12
II	4.63 ± 0.44	1.82 ± 0.78	15.5/16
III	5.03 ± 0.56	1.97 ± 0.92	20.6/17
IV	5.06 ± 0.58	1.76 ± 0.78	23.0/16

The $\vec{K}$ dependence of $R_\perp$ determines only the ratio $\frac{\beta_\perp^2}{T}$, so that a full range for the $(\beta_\perp, T)$ doublet is still conceivable. WA97 has measured the inverse m_t slope parameters T_{eff} as a function of centrality [31]. This slope can be thought as the inverse of a blue-shifted temperature $T_{eff} = T\sqrt{\frac{1+\beta_\perp}{1-\beta_\perp}}$. This relation provides a second constraint on the $(\beta_\perp, T)$ doublet range. Combining the *two*-particle correlation measurements with the *single* particle transverse mass spectra, disentangles temperature T and transverse flow $\beta_\perp$. The allowed regions in the $(T, \beta_\perp)$ parameter space, as determined by the combination of these two measurements, are shown in fig. 10, and the disentangled values for T and $\beta_\perp$ are reported in table 4.

Table 4. The freeze-out temperature T and the intensity of the transverse flow $\beta_\perp$.

Centrality	T(MeV)	$\beta_\perp$
ALL	123^{+12}_{-10}	$0.44^{+0.06}_{-0.08}$
I	140^{+26}_{-13}	$0.30^{+0.09}_{-0.16}$
II	121^{+15}_{-11}	$0.47^{+0.07}_{-0.10}$
III	117^{+16}_{-11}	$0.48^{+0.08}_{-0.11}$
IV	120^{+15}_{-11}	$0.46^{+0.07}_{-0.10}$

Postponing to the next section a global discussion about these results, we wish here to emphasize that class I features a smaller transverse freeze-out radius, a lower transverse expansion velocity and a higher temperature. This suggests an expansion on a smaller scale; the higher temperature at the freeze-out may be interpreted as the remnant of an earlier decoupling of the expanding system.

5.5. The $R_\parallel$ radius: average freeze-out proper time

In the same model of ref. [4], the dependence of $R_\parallel$ on $(K_t, Y_{\pi\pi})$ determines the average freeze-out proper time τ_0 via the formula:

$$R_\parallel = \tau_o[\frac{M_t}{T}\cosh(Y_{YK} - Y_{\pi\pi}) - \cosh^{-2}(Y_{YK} - Y_{\pi\pi}) + 1/(\Delta\eta)^2]^{-\frac{1}{2}} \qquad (7)$$

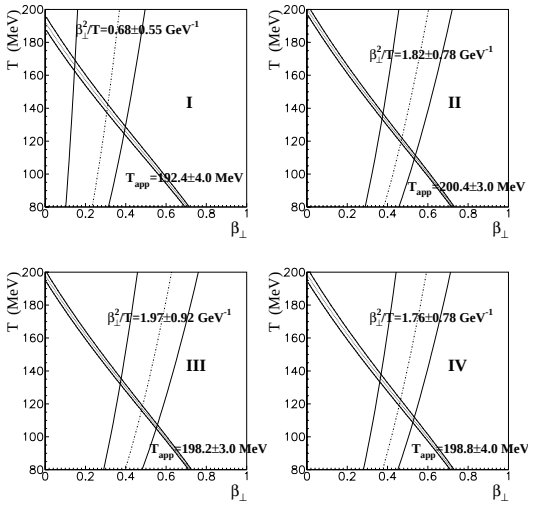

Figure 10. Allowed regions in the freeze-out temperature vs. transverse flow velocity space (see text). Bands are drawn at $\pm\sigma$ around fitted values.

The parameter $\Delta\eta$ is fixed by the extension of the single particle rapidity distribution ‡ ; it has been measured by the large acceptance NA49 experiment to be $\Delta\eta = 1.3\pm0.1$ [32]. The results of the bidimensional fits of function (7) to the experimental data are presented in table 5.

Table 5. Average freeze-out proper time τ_0 of the source.

Centrality	τ_0 (fm/c)	χ^2/ndf
ALL	5.35 ± 0.20	8.6/19
I	3.66 ± 0.22	24.3/13
II	5.08 ± 0.23	16.5/17
III	5.56 ± 0.23	20.9/19
IV	5.58 ± 0.24	9.6/17

The centrality classes III and IV show a similar behaviour, being characterized by a common mean freeze-out (proper) time $\tau_0 \simeq 5.6\,\mathrm{fm}/c$, class II presents a sligthly shorter τ_0 of about $5\,\mathrm{fm}/c$. All these values are much larger than the $3.7\,\mathrm{fm}/c$ measured for class I.

5.6. The R_0^2 parameter: mean duration of the emission

The YKP parameter R_0 is related to the mean emission duration $\Delta\tau$ of the source [33]:

$$\Delta\tau \simeq R_0 \quad \text{at high } K_t \tag{8}$$

‡ $\Delta\eta$ is related to the width of the rapidity distribution Δy by $(\Delta y)^2 = (\Delta\eta)^2 + \frac{T}{m_T}$.

As one can see for the inclusive case of *ALL* centralities shown in fig. 11, the R_0 radius does not present a significant dependence on the pair rapidity $Y_{\pi\pi}$. Therefore we have merged all the four $Y_{\pi\pi}$ bins with the aim of reducing the statistical fluctuations on the extracted R_0 when the four centrality classes are investigated separately. The R_0^2 fit

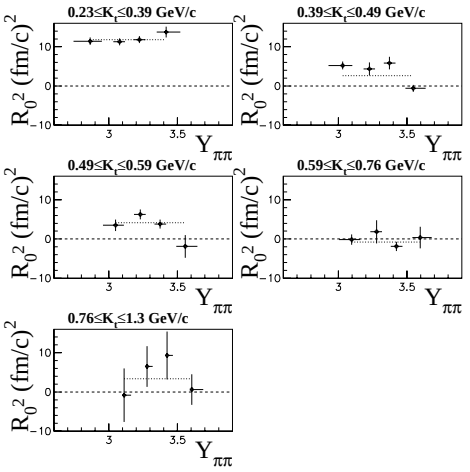

Figure 11. The R_0^2 parameter as a function of $Y_{\pi\pi}$ in five successive K_t intervals. The dotted horizontal lines through the points are the best-fit results with a constant function. The showed data refer to the case of "ALL" centralities.

results for these data sets are displayed in fig. 12 as a function of K_t.

Negative values of the R_0^2 parameter can be expected from an opaque source even at $K_\perp = 0$ [34]. In an opaque source the freeze-out occurs in the form of surface emission, as in the case of photons radiated by the sun. Fig. 12 suggests that all centrality classes are compatible with a transparent source that suddenly freezes out ($\Delta\tau \sim 0$).

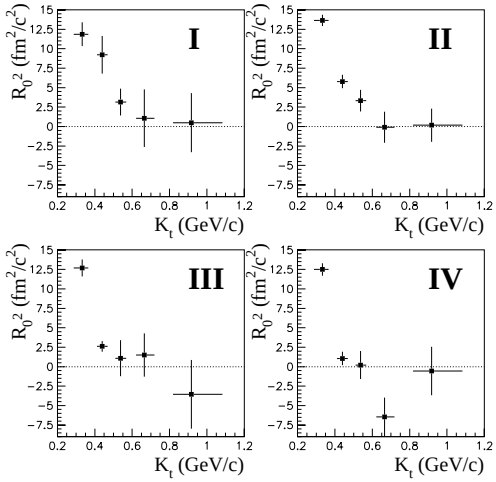

Figure 12. Dependence of R_0^2 on K_t in our full rapidity interval, for the different classes of collision centrality.

6. Discussion

The study of the $\vec{K}$–dependence of YKP parameters, combined with single-particle transverse-mass spectra, has determined several features of the source: its freeze-out temperature T, its transverse geometric (Gaussian) radius $\sqrt{2}R_G$, its average freeze-out proper time τ_0, the mean proper time duration of particle emission $\Delta\tau$, the strength of the transverse flow $\beta_\perp$, some hints on the longitudinal expansion. In table 6 we summarize the main results of this study. These data provide implicitly a dynamical picture of the collision process.

Table 6. Source parameters for the four centrality classes.

	IV	III	II	I
R_G(fm)	5.1 ± 0.6	5.0 ± 0.6	4.6 ± 0.4	3.2 ± 0.3
T(MeV)	120^{+15}_{-11}	117^{+16}_{-11}	121^{+15}_{-11}	140^{+26}_{-13}
$\beta_\perp(c)$	$0.46^{+0.07}_{-0.10}$	$0.48^{+0.08}_{-0.11}$	$0.47^{+0.07}_{-0.10}$	$0.30^{+0.09}_{-0.16}$
τ_0(fm/c)	5.6 ± 0.2	5.6 ± 0.2	5.1 ± 0.2	3.7 ± 0.2
$\Delta\tau$(fm/c)	≈ 0 at high K_t			
Long. expans.	fast			slow

With the aim of seeing if this picture is self-consistent, we can compare the two-dimensional rms width $R_{rms}^{freezeout} = \sqrt{2}R_G$ with the two-dimensional rms width of a cold lead nucleus

$$R_{rms}^{Pb} = \sqrt{\frac{3}{5}} 1.2 \mathrm{A}^{\frac{1}{3}} \simeq 4.5\,\mathrm{fm}. \tag{9}$$

For most central collisions (class III and IV), the system expands by a factor ~ 1.6 or, equivalently, by 2.65 fm in the transverse direction. If the transverse flow velocity is equal to $\beta_\perp \simeq 0.47\,c$ during the whole expansion, in a time of $\tau_0 \simeq 5.6\,\mathrm{fm}/c$ nuclear matter would travel over $\tau_0\beta_\perp \simeq 2.6\,\mathrm{fm}$ in the transverse direction. This is consistent with the previous estimate from the difference $R_{rms}^{freezeout} - R_{rms}^{Pb}$. Therefore the HBT description is internally consistent.

For less central collisions (classes I,II) the initial overlap of colliding nuclei is expected to be smaller than that given by eq.(9). A realistic estimation of such an overlap is not straightforward. However, a backward reconstruction from the data is still feasible. If the freeze-out transverse two-dimensional rms width is 4.5 fm (6.5 fm) for class I (class II), accounting for an overall expansion of $\tau_0\beta_\perp = 1.1\,\mathrm{fm}$ (2.4 fm), we may estimate the initial transverse rms width to be 3.4 fm (4.1 fm).

No quantitative description of the longitudinal expansion can be done. We can qualitatively say that the longitudinal expansion becomes stronger the more central the collisions; additionally our data would suggest a sudden step passing from centrality class I to class II (see fig. 8).

Concerning the collision time development, we have argued that the pion emission is a sudden process ($\Delta\tau \sim 0$), starting after $\sim 5.5\,\mathrm{fm}/c$ ($3.7\,\mathrm{fm}/c$) in the case of most

central (peripheral) collisions, that happens in bulk (i.e. not surface dominated). This resembles the decoupling process of photons in the Early Universe.

It can be supposed that pion decoupling is caused mostly by a rapid cooling and dilution of the baryon density. In thermal models [35] the *chemical* freeze-out temperature ($\approx$ 170 MeV), needed to describe the observed particle ratios, is considerably higher than the *thermal* freeze-out temperature. This means that the relative abundances of particle species stop changing earlier than the end of (strong) elastic collisions (thermal freeze-out). The last stage of expansion would thus be characterized by a volume dilution of baryon density without any appreciable particle recombination.

7. Conclusions

The study of two-particle correlation functions has provided valuable information both on the geometry and the dynamical state of the reaction zone at freeze-out. A Coulomb correction procedure that assumes the same model for pion emission as that used in the HBT analysis has been implemented.

We have measured both negative and positive Yano-Koonin velocities in the LCMS system at slightly forward rapidity (with respect to y_{cm}), observing a strong increase of v_{yk} with the transverse pair momentum K_t.

The simultaneous analysis of single-particle transverse mass spectra and two-particle correlation, with the help of a model that accounts for both longitudinal and transverse expansion of the source, has allowed for a reconstruction of the final freeze-out state of the source. We have measured the following parameters as a function of centrality:

- the thermal freeze-out temperature,
- the rms transverse Gaussian radius,
- the average freeze-out proper time,
- the mean proper time duration of particle emission,
- the transverse flow velocity.

From these data we have shown that our less central collision class (I) exhibits a different dynamics: the indications are that the whole expansion develops less intensely (both longitudinally and in transverse direction), the duration of expansion is shorter, the final (i.e. at freeze-out) source dimension is smaller, the system ends up with a higher temperature than in the case of more central collisions. The source parameters of the two most central collision classes (III and IV) have been found to be very similar, thus suggesting the same geometrical and dynamical freeze-out state for these classes. Class II presents parameters that are intermediate between class I and class III-IV, its dynamics being however much closer to that of classes III–IV.

Acknowledgments

We are grateful to U. Heinz, B. Tomášik and U. A. Wiedemann for fruitful discussion. We thank the NA49 and WA98 Collaborations for having provided the numerical values of their HBT radii.

REFERENCE

[1] Hanbury-Brown R and Twiss R Q 1954 *Phil. Mag.* **45** 633
[2] Goldhaber G, Goldhaber S, Lee W and Pais A, *Phys. Rev.* **178** 300
[3] Murray M 2001 *Preprint* nucl-ex/0102009
Wiedemann U A and Heinz U 1999 *Physics Reports* **319** 145
[4] Chapman S, Rayford Nix J and Heinz U 1995 *Phys. Rev.* C **52** 2694
Sinyukov Yu M 1995 *Hot Hadronic Matter: Theory and Experiment* (New York:Plenum Press)
[5] Heinz U, Tomášik B, Wiedemann U A and Wu Y -F 1996 *Phys. Lett.* B **382** 181
[6] Appelshäuser H *et al.* 1998 *The Eur. Phys. J.* C **2** 661
[7] Bamberger A *et al.* 1988 *Phys. Lett.* B **203** 320
Humanic T *et al.* 1988 *Z. Phys.* C **38** 79
[8] Alber T *et al.* 1995 *Z. Phys.* C **66** 77
Alber T *et al.* 1995 *Phys. Rev. Lett.* **74** 1303
[9] L. Rosselet *et al.* 2001 *to be published in the Proceeding of QM2001*
[10] Bearden I G *et al.* 2000 *The Eur. Phys. J.* C **18** 317
[11] Antinori F *et al.* 1995 *Nucl. Phys.* A **590** 139
[12] Andersen E *et al.* 1998 *Phys. Lett.* B **433** 209
[13] Antinori F *et al.* 2000 *The Eur. Phys. J.* C **18** 57
[14] Heijne E H M *et al.* 1994 *Nucl. Instrum. Methods* A **349** 138
Antinori F *et al.* 1995 *Nucl. Instrum. Methods* A **360** 91
[15] Bertsch G F, Gong M and Tohyama M 1998 *Phys. Rev. Lett.* C **37** 1896
[16] S. Chapman, P. Scotto and U. Heinz 1995 *Phys. Rev. Lett.* **74** 4400
[17] D. Boal, C.K. Gelbke and B.K. Jennings 1990 *Rev. Mod. Phys.* **62** 553
[18] F. Yano and S. Koonin 1978 *Phys. Lett.* B **78** 556
M.I. Podgoretskii 1983 *Sov. J. Nucl. Phys.* **37** 272
[19] J. Barrette *et al.* 1996 Nucl. Phys. A **610** 227
[20] GEANT, CERN Program Library, W5013
[21] H. Appelshäuser 1997 *Ph.D. thesis* (Frankfurt)
[22] Gamow G 1928 *Z. Phys.* **51** 204
Gurney R W and Condon E U 1929 *Phys. Rev.* **33** (1929) 204
[23] Gyulassy M, Kauffmann S K and Wilson L W 1979 *Phys. Rev.* C **20** 2267
[24] Kadija K *et al.* 1996 *Nucl. Phys.* A **610** 248
[25] Alber T *et al.* 1997 *Z. Phys.* C **73** 443
[26] Baym G and Braun-Munzinger P 1996 *Nucl. Phys.* A **610** 286
[27] Pratt S and Tsang M B 1987 *Phys. Rev.* C **36** 2390
[28] Pratt S, Csörgő T and Zimányi J 1990 *Phys. Rev.* C **54** 2646
[29] Wu Y -F, Heinz U, Tomášik B and Wiedemann U A 1998 *The Eur. Phys. J.* C **1** 599
[30] Blume C *et al.* 2001 *to be published in the Proceeding of QM2001*
[31] Antinori F *et al.* 2000 *The Eur. Phys. J.* C **14** 633
[32] Jones P *et al.* 1996 *Nucl. Phys.* A **610** 188
[33] Heinz U 1998 *Preprint* hep-ph/9806512
[34] Heiselberg H and Vischer A P 1998 *The Eur. Phys. J.* C **2** 593
Tomášik B and Heinz U 1998 *Preprint* nucl-th/9805016 *subm. to The Eur. Phys. J. C.*

[35] Beccatini F, Gaździcki M and Sollfrank J 1998 *The Eur. Phys. J.* C **5** 143